Journal of Power Sources 195 (2010) 1812–1820

Contents lists available at ScienceDirect

Journal of Power Sources

journal homepage: www.elsevier.com/locate/jpowsour

Carbon xerogels as Pt catalyst supports for polymer electrolyte membrane fuel-cell applications

Bing Liu, Stephen Creager*

Hunter Laboratory, Department of Chemistry, Clemson University, Clemson, SC 29634, United States

ARTICLE INFO

Article history:
Received 20 August 2009
Received in revised form 13 October 2009
Accepted 13 October 2009
Available online 23 October 2009

Keywords:
Carbon xerogel
Pt catalyst support
Polymer electrolyte membrane fuel cell

ABSTRACT

Carbon xerogels prepared by the resorcinol-formaldehyde (RF) sol–gel method with ambient-pressure drying were explored as Pt catalyst supports for polymer electrolyte membrane (PEM) fuel cells. Carbon xerogel samples without Pt catalyst (CX) were characterized by the N_2 sorption method (BET, BJH, others), and carbon xerogel samples with supported Pt catalyst (Pt/CX) were characterized by thermogravimetry (TGA), powder X-ray diffraction (XRD), electron microscopy (SEM, TEM) and *ex situ* cyclic voltammetry for thin-film electrode samples supported on glassy carbon and studied in a sulfuric acid electrolyte. Experiments on Pt/CX were made in comparison with commercially obtained samples of Pt catalyst supported on a Vulcan XC-72R carbon black support (Pt/XC-72R). CX samples had high BET surface area with a relatively narrow pore size distribution with a peak pore size near 14 nm. Pt contents for both Pt/CX and Pt/XC-72R were near 20 wt % as determined by TGA. Pt catalyst particles on Pt/CX had a mean diameter near 3.3 nm, slightly larger than for Pt/XC-72R which was near 2.8 nm. Electrochemically active surface areas (ESA) for Pt as determined by *ex situ* CV measurements of H adsorption/desorption were similar for Pt/XC-72R and Pt/CX but those from CO stripping were slightly higher for Pt/XC-72R than for Pt/CX. Membrane-electrode assemblies (MEAs) were fabricated from both Pt/CX and Pt/XC-72R on Nafion 117 membranes using the decal transfer method, and MEA characteristics and single-cell performance were evaluated via *in situ* cyclic voltammetry, polarization curve, and current-interrupt and high-frequency impedance methods. *In situ* CV yielded ESA values for Pt/XC-72R MEAs that were similar to those obtained by *ex situ* CV in sulfuric acid, but those for Pt/CX MEAs were smaller (by 13–17%), suggesting that access of Nafion electrolyte to Pt particles in Pt/CX electrodes is diminished relative to that for Pt/XC-72R electrodes. Polarization curve analysis at low current density (0.9 V cell voltage) reveals slightly higher intrinsic catalyst activity for the Pt/CX catalyst which may reflect the fact that Pt particle size in these catalysts is slightly higher. Cell performance at higher current densities is slightly lower for Pt/CX than the Pt/XC-72R sample, however after normalization for Pt loading, performance is slightly higher for Pt/CX, particularly in H_2/O_2 and at lower cell temperatures (50 °C). This latter finding may reflect a possible lower mass-transfer resistance in the Pt/CX sample.

1. Introduction

One of the 'quantum jumps' in polymer electrolyte fuel-cell (PEMFC) science and technology development is the jump of a 10–100-fold catalyst (Pt or Pt alloy) loading reduction in electrodes by using high-surface-area-carbon-supported catalyst instead of unsupported catalyst in the active catalyst layers in the electrodes in PEMFCs. The use of carbon-supported catalysts not only decreases significantly the production cost but also increases the catalyst (Pt or Pt alloy) utilization and thus the cell performance in fuel cells [1]. The requirements for a catalyst support for PEMFCs include the following: (1) high-surface-area; (2) suitable porosity with mainly mesopores (2–50 nm); (3) high electrical conductivity; and (4) good chemical, thermal and electrochemical stability under the harsh fuel-cell conditions (under H_2, O_2, heat, humid, acid or alkaline conditions) [2,3]. Conventionally, carbon black (e.g. Vulcan XC-72/72R from Cabot Company) is the most commonly used catalyst support in PEMFCs. Due to the importance of the catalyst support materials in fuel-cell applications, much research effort has been put on supports other than carbon blacks, such as activated carbon, carbon nanotubes, carbon nanofibers, ordered mesoporous carbons, carbon aerogels, etc. in order to discover better support materials for better fuel-cell performance and durability [2,3]. Activated carbon is very highly microporous which can result in Pt particles being trapped where they are not in contact with electrolyte or fuel, so it is expected not to be a good support candidate. Better performance on carbon nanotubes and nanofibers as supports in fuel cells has been reported, but the production cost for

* Corresponding author. Tel.: +1 864 656 2319; fax: +1 864 656 3167.
E-mail address: screage@clemson.edu (S. Creager).

0378-7753/$ – see front matter © 2009 Elsevier B.V. All rights reserved.
doi:10.1016/j.jpowsour.2009.10.033

these materials is very high which may prevent the immediate application of these supports in practice.

The structure of carbon aerogel is very different from that of carbon black. Carbon black consists of carbon agglomerates formed from weak van der Waals forces between aggregates of primary particles. The primary particles in the aggregates are fused together by strong covalent bonding. Carbon aerogel's structure can be described as three-dimensional consisting of interconnected carbon nanoparticles and interconnected nanopores. Carbon aerogel was first synthesized by Pekela [4,5] in 1989 using resorcinol (R) and formaldehyde (F) as reactants polymerized using sodium carbonate catalyst (C) to form a precursor RF hydrogel. This precursor hydrogel is then subjected to supercritical CO_2 drying and carbonization at about 1050 °C under inert atmosphere to produce the carbon aerogel. The aerogel structure (specific surface area, pore size, pore size distribution, porosity, density, etc.) can be tuned by varying synthesis conditions such as RF content in the reaction mixture (the combined weight percent of R and F relative to the weight of the overall reaction mixture including water), the ratio of C to R in the reaction mixture, pH, etc. [6,7]. Due to these special properties of carbon aerogels mentioned above, they have been pursued as gas diffusion layers [8] and as catalyst supports in the active catalyst layer [9,10] in PEMFCs. High performance of aerogels as supports in catalyst layers was reported [9], but supercritical drying is expensive and time consuming. Carbon xerogels with similar structure and properties to carbon aerogels could be prepared under ambient-pressure drying after careful control of the synthesis conditions [11–13]. The ambient-pressure drying is simple and cost-effective.

Several groups have described work using carbon aerogels and xerogels as Pt catalyst supports in PEM fuel cells [9,10,14–22]. In many cases materials have been well characterized but comparisons have not been made with conventional Pt-on-carbon black materials, and/or the materials have not been used to fabricate membrane-electrode assemblies (MEAs). In cases where MEAs were fabricated and tested, the results have been mixed. In some cases the catalysts with aerogel/xerogel supports work as well or better than conventional Pt-on-carbon black catalysts, whereas in other cases the performance is worse. Critical issues appear to include the Pt particle size and penetration of catalyst particles, electrolytes and fuels into and out of aerogel/xerogel supports. Each approach is unique and the results have varied from one group to another.

In this report, carbon xerogels with BET surface area of 460 $m^2\ g^{-1}$ and peak pore size 14 nm were produced by modifying a previously described ambient-pressure drying method [12,13] and explored as Pt catalyst supports for H_2/O_2 (air) PEMFCs. The carbon xerogel supported Pt catalysts (Pt/CX) were characterized by thermogravimetry (TGA), powder X-ray diffraction (XRD), electron microscopy (SEM, TEM) and *ex situ* cyclic voltammetry for thin-film electrode samples supported on glassy carbon and studied in a sulfuric acid electrolyte. Pt/CX samples were studied in comparison with commercially obtained samples of Pt catalyst supported on a Vulcan XC-72R carbon black support (Pt/XC-72R). The Pt/CX samples were also used to fabricate MEAs which were tested in a single-cell test station.

2. Experimental

2.1. Synthesis of carbon xerogel

Carbon xerogels were synthesized by the RF sol–gel method using ambient-pressure evaporative drying [12,13]. The R/F mole ratio was kept at 1:2 and C/R mole ratio was at 1:1500. The RF content was 30 wt%. A typical preparation proceeded as follows: calculated amounts of resorcinol (98%, Aldrich) and formaldehyde (37 wt%, ACS Reagent, Aldrich) were mixed in a glass test tube (approximately 50 mL) with DI water using sodium carbonate as polymerization catalyst. The solution pH was adjusted to near 7 before the test tube was sealed with a rubber septum. The sol was cured at room temperature, 50 and 90 °C, 1 day each, then the gel was exchanged with acetone three times to remove water from inside the pores. The acetone-filled RF gel was then dried in air. Finally the carbon xerogel product was obtained after carbonizing the dried organic RF gel at 1050 °C under flowing N_2 for 4 h.

2.2. Catalyst deposition onto carbon xerogel

Carbon aerogel (CX) samples (about 0.1 g) were ground in an agate mortar to a fine powder, and the resulting powders were sonicated in 30 mL DI water for 15 min. Then, a diluted H_2PtCl_6 (Acros Organics, 40% Pt) solution was added into the carbon powder suspension and sonicated for another 30 min. The mass of platinum salt added to the CX sample corresponded to 20 wt% of platinum metal in the final material. After sonication, the mixture pH was adjusted to 11 and an excess amount (10×) of formaldehyde was diluted in DI water (2 mL) and added drop by drop into the carbon suspension under stirring. The mixture was kept stirring for another 15 min at room temperature, then the reaction temperature was raised to 90 °C and kept at 90 °C for 2 h under stirring. Then the reaction was cooled down to room temperature and diluted HCl (2 mol L^{-1}) was added to promote precipitation of Pt catalyst onto carbon powders. The Pt-deposited carbon xerogel powder (Pt/CX) was then filtered, thoroughly washed with DI water, and dried at 100 °C under vacuum. For all Pt/CX samples subjected to further analysis, the final Pt content was approximately 20 wt% as measured by thermogravimetric analysis (TGA) under O_2 atmosphere.

2.3. Characterization of the materials

2.3.1. N_2 adsorption/desorption method

The specific surface area and pore texture of the carbon xerogels were characterized by the analysis of nitrogen adsorption–desorption isotherms, performed at 77 K with a Micromeritics ASAP 2010 apparatus. The sample was degassed at 200 °C for 1 day before measurement. The specific surface area (S_{BET}) of carbon xerogel samples was obtained using the Brunauer–Emmett–Teller (BET) model [23], micropore properties (microporous volume V_{micro}, microporous surface area S_{micro}) were obtained using the *t*-plot method [24,25] and the Barrett–Joyner–Halenda (BJH) model [26] was used to evaluate the mesopore properties (mesoporous volume V_{meso}, mesoporous surface area S_{meso} pore size and distribution (PSD). The total pore volume (V_{total}) was recorded at P/P_0 of near saturation. As a comparison, a commercial support Vulcan XC-72R from Cabot Company (without Pt) was also characterized by the N_2 adsorption/desorption method.

2.3.2. Powder X-ray diffraction (XRD)

X-ray powder diffractograms of Pt/CX and Pt/XC-72R (20% Pt, Alfa Aesar) samples were obtained using a Scintag XDS2000 powder x-ray diffractometer using Cu Kα radiation of wavelength 0.1540 nm. The 2θ angular range between 5° and 90° was scanned at 0.5 s per step in 0.02° steps.

2.3.3. Electron microscopy

Scanning electron microscopy (SEM) measurements on Pt/CX samples were performed using a Hitachi S-4800 microscope equipped with an Oxford INCA EDS detector. Pt mapping was done with EDS. The powder sample was mounted on a double-sided carbon sticky tape. Transmission electron microscopy (TEM) measurements were performed on Pt/CX and Pt/XC-72R samples using a Hitachi H7600T transmission electron microscope which was

operated at an accelerating voltage of 200 kV. The samples were prepared by dispersing a small amount of the catalyst powder in ethanol with ultrasonic treatment. Several drops of the dispersion were taken using a pipette and put on a holey carbon copper grid, followed by drying in air at room temperature overnight.

2.3.4. Thermogravimetry analysis (TGA)

The Pt contents of Pt/CX and Pt/XC-72R samples were determined from the residual mass following TGA under O_2 atmosphere at 850 °C with a heating rate of 15 °C min^{-1} using a Mettler Toledo TGA/SDA 851e analyzer. Residual mass for Pt-containing samples is assumed to be Pt metal. TGA runs on Pt-free carbon samples showed very low residual masses (<1%).

2.3.5. Ex situ cyclic voltammetry and CO stripping voltammetry

Ex situ cyclic voltammetry (CV) was employed to characterize the electrochemically active surface area (ESA) of Pt catalysts. CV measurements were made using a CH Instruments model 660A electrochemical with a standard three-electrode cell with home-made Hg/Hg_2SO_4 (0.1 mol L^{-1} H_2SO_4) reference and Pt wire counter electrodes. The working electrode was a freshly cleaned glassy carbon (GC) plate electrode onto which a thin layer electrode was formed by evaporation of 10 μL of a well-mixed ink suspension consisting of supported catalyst and solubilized Nafion solution in isopropanol (0.5 mL isopropanol, 10 mg Pt/C catalyst, and 50 mg 5% Nafion (EW 1100, Solution technology) mixed together and stirred overnight). *Ex situ* CV measurements were performed by partial immersion of the GC electrode in 0.5 mol L^{-1} deaerated H_2SO_4 solutions with N_2 blanket on the top. Before recording the CVs used to determine ESA, the potential was repeatedly cycled until a stable voltammogram was obtained. In the case of CO stripping, electrodes were exposed to CO by brief bubbling with CO gas with the electrode held at −0.25 V (vs. Hg/Hg_2SO_4) prior to voltammetric analysis.

2.3.6. MEA fabrication

Membrane-electrode assemblies (MEAs) were prepared using the decal transfer method developed by Wilson and co-workers [27,28]. In brief, an ink was prepared by mixing carbon-supported catalyst (20% Pt/CX, or 20% Pt/XC-72R), solubilized Nafion solution (5%, EW 1100), isopropanol, glycerol and tetrabutyl ammonium hydroxide solution (1 M in methanol, Aldrich) with a dry mass ratio of Pt/carbon to Nafion of 5:2. The ink was applied via several steps of painting thin layers of ink onto Teflon-coated fiberglass templates followed by heating at 140 °C for 30 min to remove solvent, to achieve a Pt catalyst loading in the range of 0.25 mg cm^{-2}. An MEA was then made by hot-pressing a Nafion 117 membrane in Na^+ form with two ink-coated templates (one on each side) at 200–210 °C and 600 lbs force for 5 min. Following hot-pressing, the MEA was boiled in 0.5 mol L^{-1} sulfuric acid for 1 h to convert all ionomer back to the proton form, then boiled in DI water for 1 h and washed with DI water several times. The MEAs were stored in DI water before use.

2.3.7. Single fuel-cell testing

The single-cell testing of MEAs was performed on a model 850C test station from Scribner Associates Company. Before assembling in the test fixture, the MEA was pulled dry and flat on a vacuum table at 60 °C for 20 min, and then the MEA was mounted on the test fixture by sandwiching the MEA between the two pieces of uncatalyzed gas diffusion backing (ELAT/NC, E-TEK). The active area of an MEA is 5 cm^2. Humidified fuel (H_2) and oxidant (O_2 or air) gases were supplied to the test fixture by the test station. The cell was operated under ambient pressure on both the anode and cathode. Cells were broken in at a cell voltage of 0.5 V overnight, after which a series of polarization curves was acquired in controlled voltage mode under different operating conditions. The cell open circuit voltage (OCV) was close to or above 1.0 V for all MEAs. The cell resistance was monitored during acquisition of the polarization curves using the current-interrupt method (CI) and by high-frequency impedance spectroscopy (HFR) at 1 kHz frequency [29].

2.3.8. In situ MEA cyclic voltammetry

The *in situ* CV measurement was used to obtain ESA values for the supported Pt catalysts in the MEAs in the fuel-cell test fixture [30]. For such a measurement the fuel-cell station operated in a two-electrode configuration in which the anode severed as both pseudo-reference and counter electrodes, and the cathode served as the working electrode. The anode was fed with high purity H_2 gas (humidified) and the cathode was fed with high purity N_2 gas (humidified). The gas flow of both N_2 and H_2 was kept at 50 mL min^{-1} during the measurements. Solartron 1280B electrochemical unit was used as a potentiostat. The potential was cycled between 0 and 0.8 V with a scan rate of 40 mV s^{-1}.

3. Results and discussion

The CX samples synthesized as described above were characterized via their N_2 adsorption and desorption isotherms in comparison with the commercial carbon black support Vulcan XC-72R (which was used as the catalyst support for the commercially obtained Pt/XC-72R samples). The N_2 adsorption and desorption isotherms are shown in Fig. 1. The CX sample shows a type IV, H2 isotherm according to IUPAC classification [31] indicating that mesopores exist in the sample. The pore size distribution (PSD) deduced from the BJH method for both CX and XC-72R samples is shown in Fig. 2. The CX sample has a relatively sharp pore size distribution, with pore sizes between 5 and 30 nm while XC-72R carbon shows a broad PSD of about 2–300 nm. The XC-72R broad PSD was reported in literature and reflects its aggregate and agglomerate structure. Other textural properties of CX and XC-72R are listed in Table 1. From Table 1 it is seen that CX has nearly double the BET surface area of XC-72R while the mesoporosity (V_{meso}/V_{total}) for both samples is nearly the same. The CX sample has more micropore surface area (higher S_{micro}/S_{BET}) although for both supports, the micropore volume is low.

The Pt catalyst was deposited onto CX powder samples by the impregnation–reduction method using hexachloroplatinic acid as a Pt precursor and formaldehyde as a reducing agent [32,33]. TGA analysis showed the Pt contents in most Pt/CX samples were close

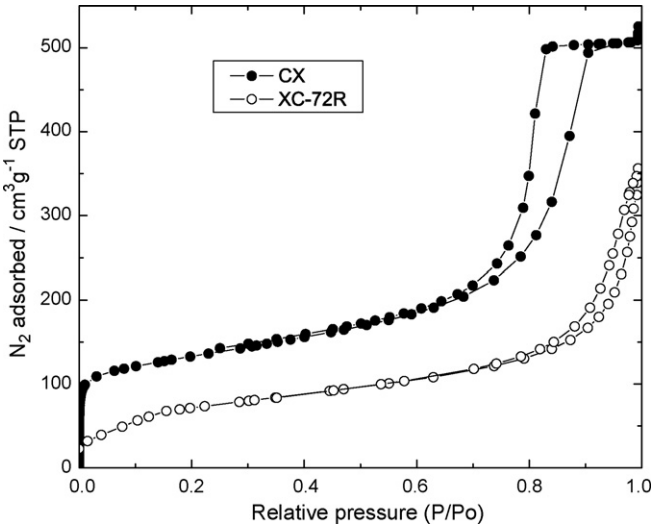

Fig. 1. The N_2 sorption isotherms of carbon xerogel (CX) (●) and XC-72R (○).

Table 1
Textural property of carbon xerogel and carbon black.

Carbon	S_{BET} ($m^2\ g^{-1}$)	S_{micro} ($m^2\ g^{-1}$)	S_{micro}/S_{BET}	V_{total} ($cm^3\ g^{-1}$)	V_{micro} ($cm^3\ g^{-1}$)	V_{meso} ($cm^3\ g^{-1}$)	V_{meso}/V_{total}	d_{BET} (nm)	d_{BJH_ads} (nm)	d_{BJH_des} (nm)
CX	462	197	0.43	0.81	0.09	0.70	0.86	7.0	10.4	9.9
XC-72R	237	83	0.35	0.62	0.04	0.55	0.89	10.4	17.6	22.7

S_{BET}: BET surface area; S_{micro}: micropore surface area by *t*-plot; V_{total}: total pore volume at near saturation pressure; V_{meso}: cumulative volume of pores between 1.7 and 300 nm by BJH adsorption branch; d_{BET}, d_{BJH_ads}, d_{BJH_des}: average pore width by 4 V/A.

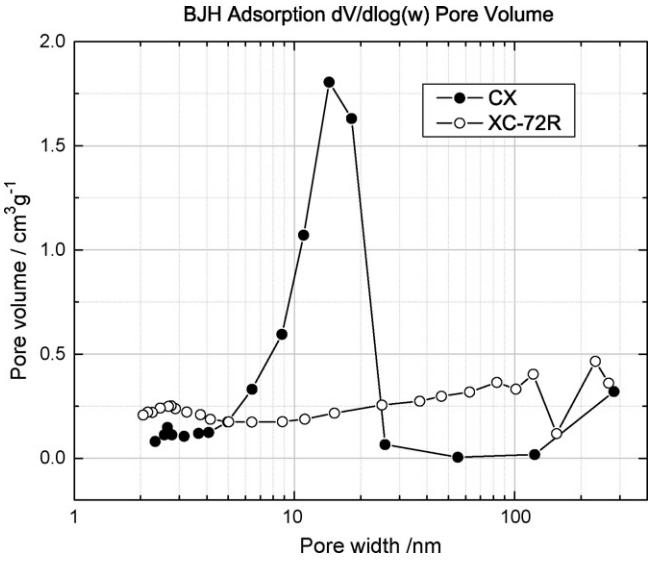

Fig. 2. The pore size distribution of carbon xerogel (CX) (●) and XC-72R (○).

to the 20 wt% value expected from the amount of hexachloroplatinic acid used in the Pt deposition step. This finding confirms that Pt reduction/deposition proceeds with high efficiency.

The Pt/CX samples were subjected to powder XRD analysis to confirm Pt deposition and allow for estimation of Pt particle sizes. The XRD graphs of a representative Pt/CX sample and a commercial Pt/XC-72R sample are shown in Fig. 3. The diffractogram shows features expected for Pt as labeled on the graph; the feature near 25° 2θ is from the carbon substrate. The Pt diffraction lines are generally narrower for the Pt/CX sample relative to the Pt/XC-72R sample, which suggests that the Pt particles on the Pt/CX sample are larger.

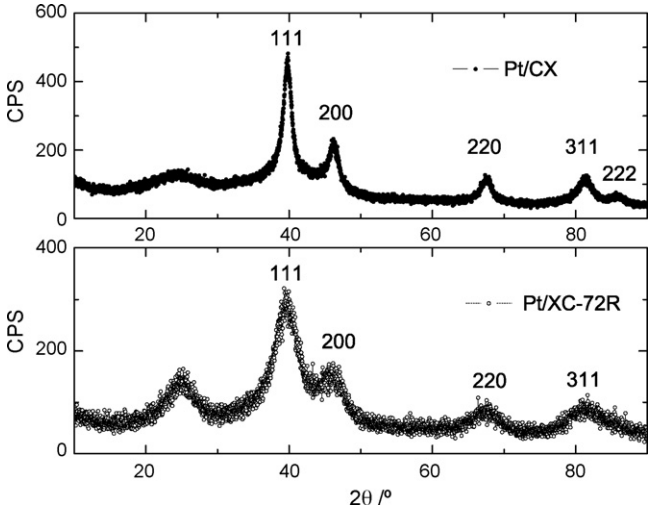

Fig. 3. XRD graphs of carbon-supported catalysts Pt/CX (top) and Pt/XC-72R (bottom).

Nanoparticle sizes may be quantified from powder XRD data using the Scherer equation. For the case of Pt-on-carbon it is common to use the Pt(2 2 0) line for this analysis. According to the Scherer equation (Eq. (1)) [34], from the line broadening of the Pt crystal face 2 2 0 [35], the Pt particle size may be estimated.

$$d(\text{nm}) = \frac{0.9\lambda}{B\ \cos(\theta)} \quad (1)$$

In this equation d is the Pt crystal size (diameter), λ is the X-ray wavelength (0.1540 nm), B is the full width at half height for the diffraction peak in radians and θ is half of the diffraction angle. Particle size values obtained in this way for Pt/CX and Pt/CX-72R are given in Table 2. As expected, Pt particle diameters are higher for the Pt/CX sample (4.5 nm) than the Pt/XC-72R (2.2 nm).

From the particle size obtained as described above, the Pt specific surface area may be calculated using Eq. (2):

$$S(\text{m}^2\ \text{g}^{-1}) = \frac{6000}{\rho d} \quad (2)$$

In this equation d is the Pt particle diameter (nm), and ρ is the Pt density (21.4 g cm^{-3}). Pt specific surface areas calculated in this way are listed in Table 2 for Pt/CX and Pt/XC-72R samples. These values will be compared with Pt specific surface area values obtained from TEM estimates of Pt particle size, and also with ESA values obtained by *ex situ* and *in situ* CV measurements.

An SEM micrograph and Pt map (by EDX) of a Pt-deposited carbon xerogel sample are seen in Fig. 4. The ground CX sample consists of a broad range of particle sizes, from submicron to several tens of microns. This finding is in sharp contrast to carbon black supports which are generally very fine powders. The Pt spatial distribution on the CX supports is shown in the Pt EDX map to be relatively homogeneous on the length scale shown in the figure. The Pt/CX powder samples were ground a second time before using them to make the catalyst ink for MEA fabrication, and also the thin-film electrodes used for *ex situ* CV experiments. This was done to make the MEA active layers more homogeneous and thin.

Transmission electron microscopy (TEM) was used to characterize catalyst supports on a much finer length scale than SEM, and to provide an alternate estimate of Pt particle size. The TEM micrographs and the histogram graphs of Pt particle size for the Pt/CX and Pt/XC-72R samples are shown in Figs. 5 and 6 respectively. The micrograph for Pt/XC-72R shows the typical structure expected for carbon black of aggregates of small carbon primary particles. The Pt/CX sample does not show this structure; rather it consists of larger regions of porous carbon. Lower magnification TEM micrographs (not shown) support this view of the CX samples as consisting of relatively large particles with internal porosity. Both TEM micrographs also clearly show the supported Pt particles. In both cases but particularly for the Pt/CX sample, the Pt particles appear to be distributed all throughout the carbon support, and not just on the carbon particle surface. The mean Pt diameter for Pt/CX and Pt/XC-72R samples is estimated to be 3.3 ± 1.1 and 2.8 ± 0.7 nm respectively by counting more than 200 particles from each TEM image using ImageJ software [36]. Error estimates are standard deviations from which a slightly broader Pt size distribution for Pt/CX is seen. The specific surface area (SA) of Pt could be calculated according to Eq. (2) from the Pt particle size measured by TEM or XRD on the Pt/CX and Pt/XC-72R samples, and the val-

Table 2
Pt nanoparticle size and specific surface area by different methods (XRD, TEM, *ex situ* CV (H), *ex situ* CV (CO) and *in situ* CV (H).

Sample	d_{XRD} (nm)	S_{XRD} ($m^2\,g^{-1}$)	d_{TEM} (nm)	S_{TEM} ($m^2\,g^{-1}$)	S_H ($m^2\,g^{-1}$)	S_{CO} ($m^2\,g^{-1}$)	$S_{in\,situ}$ ($m^2\,g^{-1}$)
Pt/CX	4.5	62.3	3.3	85	67	63	55
Pt/XC-72R	2.2	127.4	2.8	100.1	67	66	65

d_{XRD}: particle size by XRD; d_{TEM}: particle size by TEM; S_{XRD}, S_{TEM}: the specific surface area calculated from Eq. (2) from XRD and TEM respectively; S_H: specific surface area from *ex situ* CV (H desorption charge); S_{CO}: surface area from *ex situ* CO stripping CV; $S_{in\,situ}$: surface area from *in situ* CV (in MEA).

ues are listed in Table 2 in comparison with the ESA measured by *ex situ* and *in situ* CVs. Pt specific SA of Pt/CX is smaller than that of Pt/XC-72R due to smaller Pt particle size on Pt/XC-72R. Usually the Pt catalyst specific surface area from TEM and XRD are larger than that measured by *ex situ* or *in situ* CV because TEM or XRD measurement includes electrochemically inaccessible Pt particle. Also the ESA measured *ex situ* (in a half cell) is commonly higher than that measured *in situ* (in a full cell) due to better ion conduction by help from free acid (H_2SO_4) in the half-cell measurement. These would be seen in following discussion.

Ex situ CV is commonly used to estimate electrochemically active Pt surface area (ESA) for comparison with areas calculated from Pt particle sizes. Estimates may be obtained from H adsorption/desorption or CO stripping. For the case of H adsorption/desorption, the ESA (S_{ESA}, $m^2\,g^{-1}$ Pt) may be calculated from Eq. (3) [37]:

$$S_{ESA}(m^2\,g^{-1}\,Pt) = 100 \times \frac{q}{\Gamma L_{Pt}} \quad (3)$$

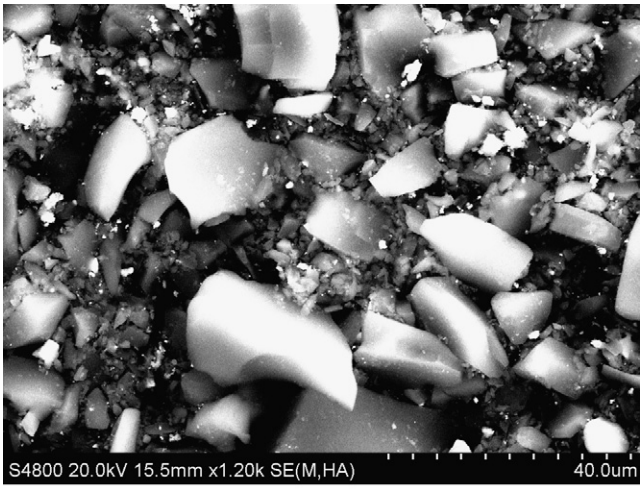

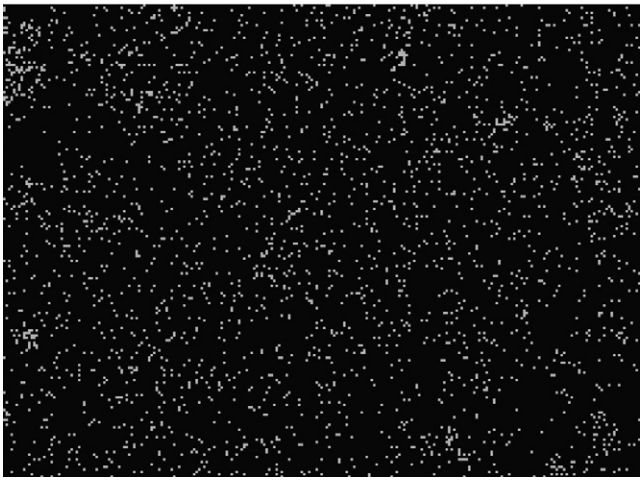

Fig. 4. SEM micrograph and Pt mapping of Pt/CX, top: SEM, bottom: Pt map (white spot: Pt particle).

In this equation q is the hydrogen adsorption or desorption charge density determined by CV ($mC\,cm^{-2}$), Γ ($210\,\mu C\,cm^{-2}$) is the well-established quantity for the charge to reduce a monolayer of protons on Pt, L_{Pt} is the Pt loading in the electrode ($mg\,cm^{-2}$). Fig. 7(left) presents CVs for Pt/CX and Pt/XC-72R samples for the H adsorption or desorption region. The CV shapes are as expected for Pt-on-carbon. Estimates of the hydrogen adsorption or desorption charge density were made as described in Refs. [37,38], and ESA values are given in Table 2. Somewhat surprisingly, ESA values are nearly identical for the two samples despite previous findings that Pt particles sizes are smaller for the Pt/XC-72R sample. We believe that this finding reflects the possible presence of Pt particles in micropores of the Pt/XC-72R sample that may be inaccessible to even liquid electrolyte. It is possible that Pt particles did not enter into micropores in the Pt/CX sample due to the technique used to make Pt particles and deposit them.

Fig. 7(right) shows *ex situ* CVs for CO stripping for Pt/CX and Pt/XC-72R samples. ESA values were again obtained using Eq. (3) but with a Γ value of ($420\,\mu C\,cm^{-2}$) [37] which is appropriate for CO stripping. ESA values from CO stripping are in relatively good agreement with those from hydrogen adsorption or desorption (i.e. agreement to within 10% which is as good as can be expected given the uncertainties associated with baseline subtraction in CV integration, sample weighing and volume measurement by micropipette), which serves to validate both methods. We note that the onset and peak potentials for CO oxidation are shifted slightly negative for Pt/CX relative to Pt/XC-72R. This shift is consistent with expectations if the Pt particles are slightly larger in the Pt/CX catalyst [39].

In situ CV may be used to estimate Pt ESA in intact electrodes in MEAs. Comparison of ESAs for such samples with those obtained by *ex situ* CV provides information on catalyst utilization in the MEA. Generally, the cathode is of most interest because of the sluggish reaction kinetics of the oxygen reduction. *In situ* CV (Fig. 8) yielded ESA values for Pt/XC-72R cathodes that were similar to those obtained by *ex situ* CV in sulfuric acid, suggesting that Pt utilization is high in these electrodes (notwithstanding the comment above regarding the possible presence of Pt trapped in micropores in Pt/XC-72R which would be inaccessible to both *in situ* and *ex situ* CV). In contrast, *in situ* CV (Fig. 8) for Pt/CX cathodes revealed a smaller ESA value, e.g. $55\,m^2\,g^{-1}$, than was obtained by *ex situ* CV, e.g. 63–67 $m^2\,g^{-1}$. This finding suggests that access of Nafion electrolyte to Pt particles in Pt/CX electrodes is diminished relative to that for Pt/XC-72R electrodes.

MEAs fabricated with both Pt/CX and Pt/XC-72R catalysts were tested at 50 and 80 °C in both H_2/O_2 and H_2/air cells under atmospheric pressure conditions. The polarization and resistance curves are shown in Figs. 9 and 10 respectively. In the following discussion we consider two ways of analyzing these data. In one approach we consider performance at high cell voltage (0.9 V) and low current density, where current is limited principally by the catalyst intrinsic activity. This approach allows for quantitative comparison of catalyst intrinsic activity with published values for related catalysts. The second approach focuses on performance at higher current density and lower cell voltage. These conditions are closer to those under which a cell would operate in a real-world application. Comparison of performance under these two conditions allows for a more

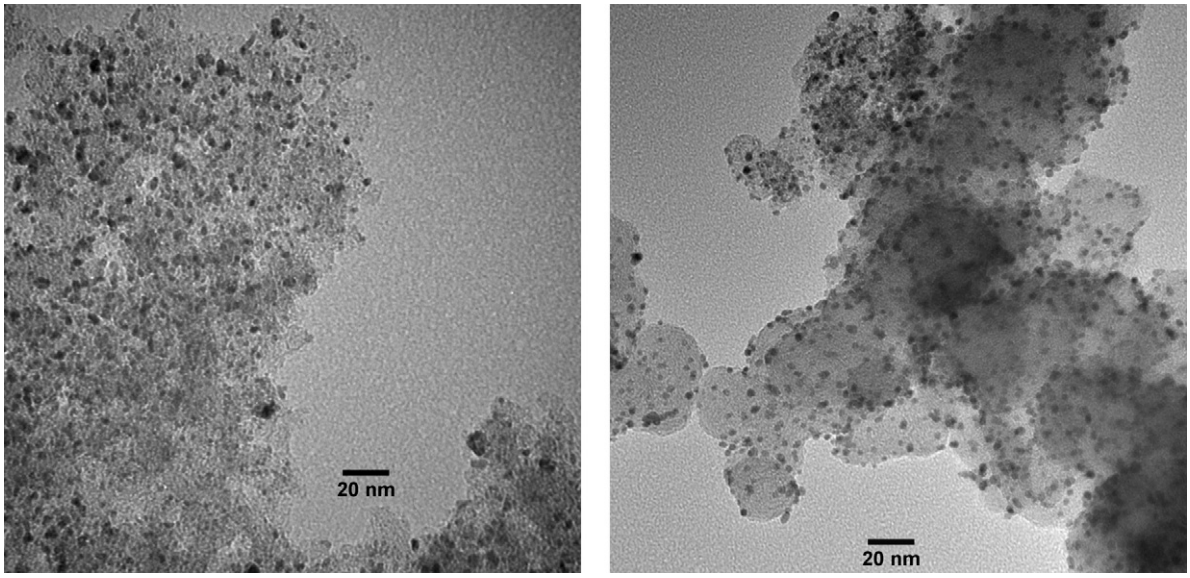

Fig. 5. TEM micrographs of Pt/CX (left) and Pt/XC-72R (right).

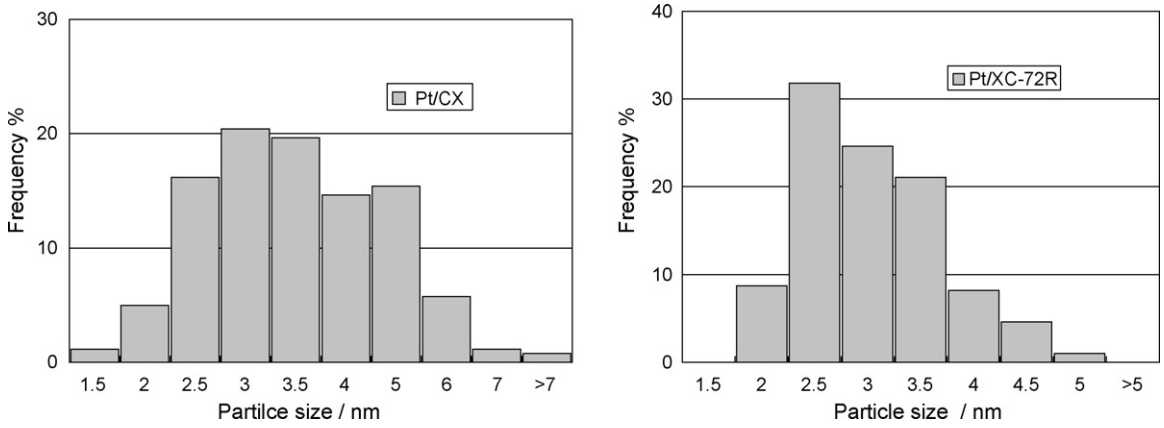

Fig. 6. Pt Particle size histogram of carbon-supported catalysts by TEM, Pt/CX (left, $d_{mean} = 3.3 \pm 1.1$ nm), and Pt/XC-72R (right, $d_{mean} = 2.8 \pm 0.7$ nm),

careful consideration of loss mechanisms under different operating conditions.

Table 3 presents values for the intrinsic catalyst activity for Pt/CX and Pt/XC-72R cathodes at 80 °C in H_2/O_2 cells at 100% RH at atmospheric pressure. Values are given for both area-normalized and mass-normalized activity at 0.9 V cell voltage which follows the recommended procedure for comparing intrinsic catalyst activities under conditions where ohmic and mass-transfer limits should

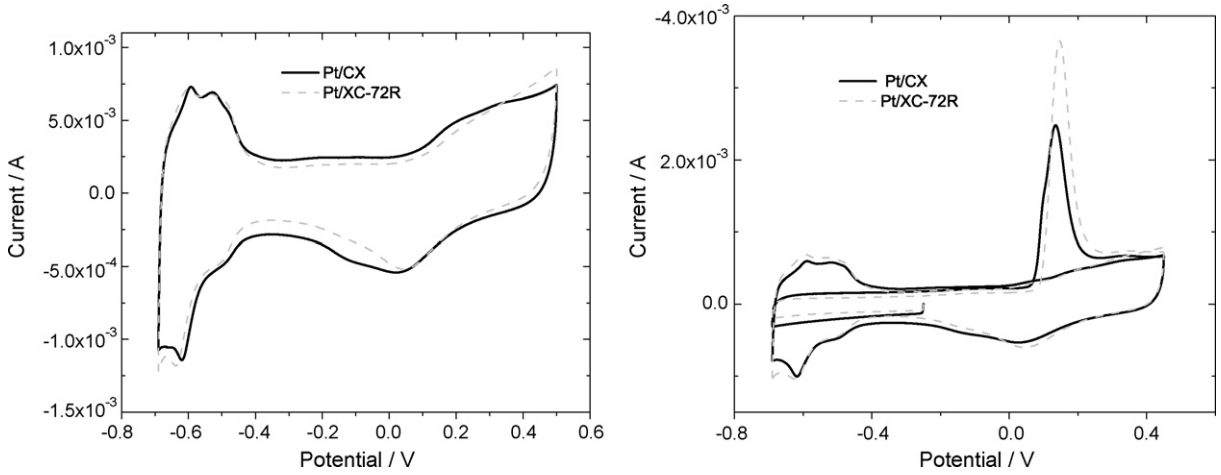

Fig. 7. *Ex situ* CVs (left) and CO stripping CVs (right) of Pt/CX (solid line) and commercial Pt/XC-72R (dash line), WE: thin-film-catalyst coated GC, RE: Hg/Hg_2SO_4, CE: Pt wire; scan rate: 20 mV s^{-1}.

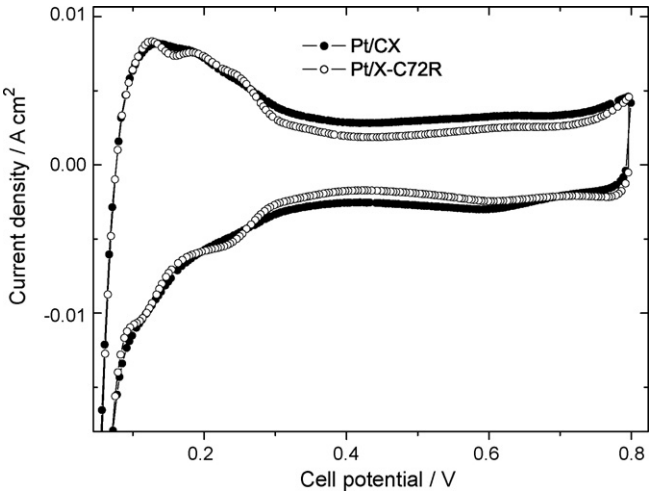

Fig. 8. *In situ* CVs of Pt/CX and commercial Pt/XC-72R catalysts; anode: H_2, 50 ml min^{-1}; cathode: N_2, 50 ml min^{-1}; cell temperature, 30 °C; potential range, 0–0.8 V; scan rate, 40 mV s^{-1}.

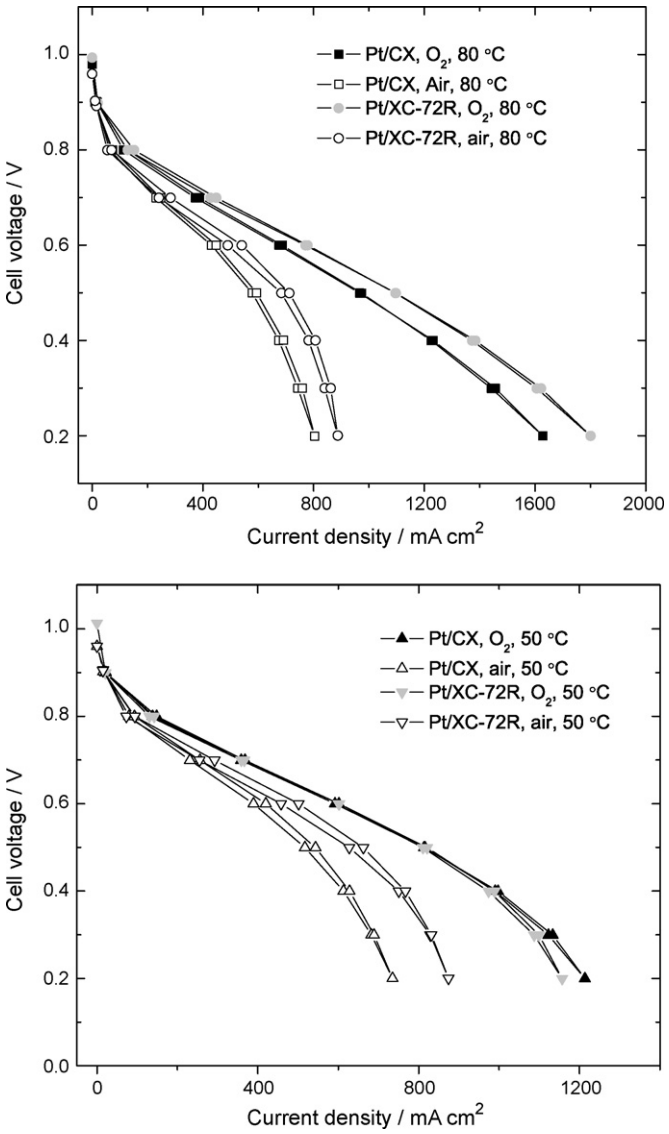

Fig. 9. Polarization curves of MEAs tested in H_2/O_2 or H_2/air cells, at 80 °C (top) and at 50 °C (bottom). Measurement conditions: H_2/O_2 or air, cell temperature 80 or 50 °C, stoichiometric ratio, H_2 1.25, O_2 1.5, or air 4.0, all measurements at atmospheric pressure, and Pt loading around 0.25 mg cm^{-2} in both anode and cathode.

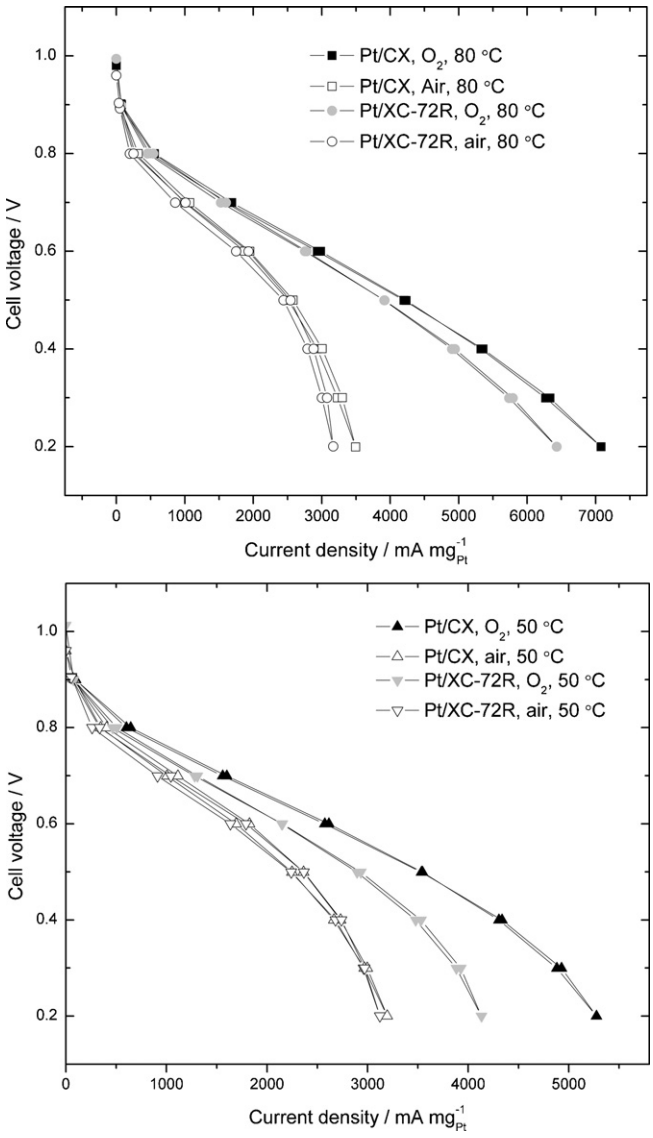

Fig. 10. Polarization curve data from Fig. 9 with currents normalized to Pt loading.

be minimized [40,41]. The lower values are without correction for the oxygen partial pressure (which is less than 1 atm due to the partial pressure of water vapor) and the higher values are after correction for the contribution of water partial pressure, assuming first-order dependence of current on oxygen partial pressure. Comparison with literature values shows that these catalysts have quite high activities. For example Gasteiger et al. [40] have suggested that an area-specific activity of 170–210 μA cm^{-2} Pt is a good benchmark for comparison with new catalysts, and both our catalysts exceed this value. Significantly, the area-specific activity for the Pt/CX catalyst exceeds that of the Pt/XC-72R catalyst by approximately 20%. This finding is consistent with the fact that the Pt/CX catalyst has a slightly larger Pt particle size. Larger Pt particles have been shown to give higher area-specific activities.

We next consider the cell performance at lower cell voltages, near 0.3–0.6 V, where current densities are much higher, e.g. by up to 80 times, and mass-transfer limitations are more prevalent. The performance of Pt/CX cells in H_2/O_2 at 80 °C (as indicated by current density at a particular cell voltage) is slightly poorer than that of Pt/XC-72R. The performance of Pt/CX in H_2/O_2 at 50 °C is close to that of Pt/XC-72R while performance in H_2/air at both 50 and 80 °C is poorer. Performance under such conditions is affected by many

Table 3
Specific activity $I_{s(0.9\,V)}$ and mass activity $I_{m(0.9\,V)}$, of Pt/CX and Pt/XC-72R catalysts at 80 °C, H_2/O_2, 100% RH, atmospheric pressure.

Sample	ESA *in situ* ($m^2\,g^{-1}$)	Pt loading ($mg_{Pt}\,cm^{-2}$)	$I_{(0.9\,V)}$ ($mA\,cm^{-2}$)	$I_{s(0.9\,V)}$ ($\mu A\,cm^{-2}$ Pt)	$I_{m(0.9\,V)}$ ($mA\,mg^{-1}$ Pt)	$I_s^*(0.9\,V)\,100\,kPa$ ($\mu A\,cm^{-2}$ Pt)	$I_m^*(0.9\,V)\,100\,kPa$ ($mA\,mg^{-1}$ Pt)
Pt/CX	55	0.23	17.3	136	75	259	143
Pt/XC-72R	65	0.28	19.7	108	70	206	134

$I_s^*(0.9\,V)\,100\,kPa$ and $I_m^*(0.9\,V)\,100\,kPa$ values are after correction for the oxygen partial pressure which were made assuming a first-order dependence of cell current on oxygen partial pressure and a water partial pressure of 47.37 kPa which corresponds to saturation conditions at 80 °C and 100% RH.

factors, one of which is Pt loading, and it is instructive to compare performance curves following normalization for Pt loading. Fig. 10 presents the data from Fig. 9 with just this normalization applied. It is clear that under all conditions, but especially in H_2/O_2 at lower temperature, performance of the Pt/CX cell is slightly better than that of the Pt/XC-72R cell. We believe that this slightly improved performance of the Pt/CX cell under these higher current density conditions reflects a lower mass-transfer resistance in the Pt/CX catalyst.

The curves of areal resistance vs. current density of MEAs made with Pt/CX and Pt/XC-72R are shown in Fig. 11. The areal resistance for Pt/CX is slightly lower than that of Pt/XC-72R although Pt/XC-72R has the higher currents (see Fig. 9). Because the two MEAs were tested using similar Nafion 117 membranes, the resistance difference should be caused by the active catalyst layer and not the membrane. This finding may therefore indicate a lower electrical contact resistance between the membrane and the catalyst layer in the Pt/CX sample.

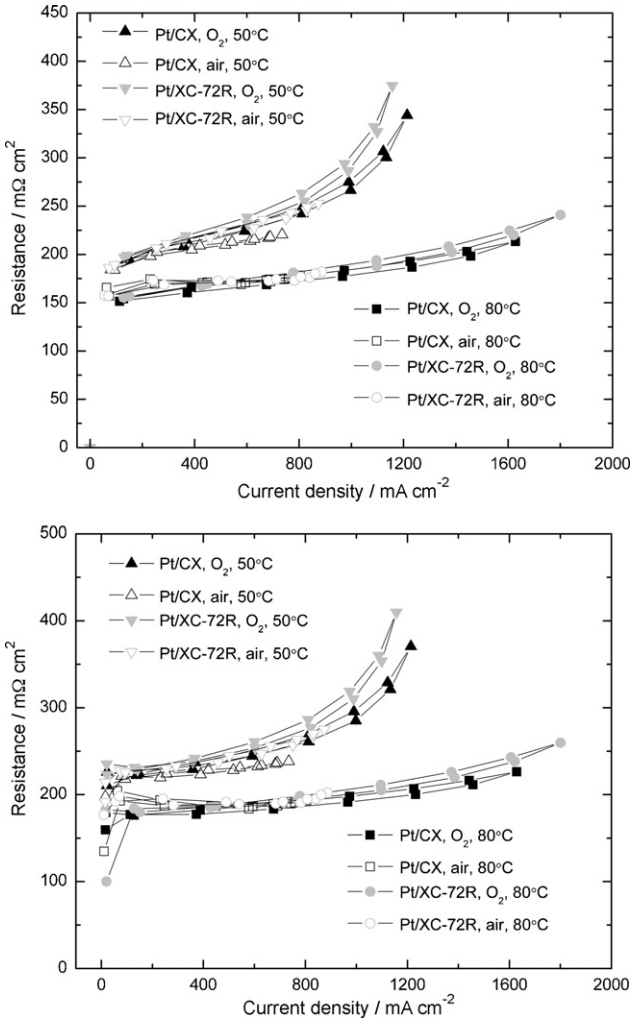

Fig. 11. Resistance of the carbon-supported catalysts by CI (top) and HFR (bottom) methods, measurement conditions same as that in Fig. 9, for HFR, frequency at 1 kHz.

4. Conclusions

Carbon xerogel with high-surface-area and a peak pore size 14 nm was synthesized by the RF sol–gel method using ambient-pressure drying and explored as a catalyst support for polymer electrolyte fuel cells in comparison with a commercial carbon black XC-72R-supported catalyst. Both catalysts were characterized with XRD, SEM, TEM, cyclic voltammetry both *ex situ* (thin-film electrode supported on glassy carbon and immersed in electrolyte) and *in situ* (in an MEA). The Pt/CX catalyst was shown to have slightly higher Pt particle sizes, slightly lower accessibility of Pt particles to Nafion electrolyte, and slightly higher intrinsic catalytic activity at 0.9 V cell voltage when normalized to Pt area. Cell performance at lower cell voltages/higher current densities was slightly lower for a Pt/CX MEA than for a Pt/XC72R MEA, however performance was slightly higher following normalization for Pt loading. This finding may reflect a lower mass-transfer resistance within the pores of the Pt/CX sample.

Acknowledgements

The authors are grateful to Dr. Don VanDerveer for assistance with XRD measurements, and to the staff of the Clemson University Electron Microscopy lab for assistance with EM measurements. The authors gratefully acknowledge the US Department of Energy Basic Energy Sciences program (award number DE-FG02-05ER15718) for financial support of this work.

References

[1] P. Costamanga, S. Srinivasan, J. Power Sources 102 (2001) 242–252.
[2] H. Liu, C. Song, L. Zhang, J. Zhang, H. Wang, D.P. Wilkinson, J. Power Sources 155 (2) (2006) 95–110.
[3] A.L. Dicks, J. Power Sources 156 (2) (2006) 128–141.
[4] R.W. Pekala, F.M. Kong, Polym. Prepr. 30 (1989) 221.
[5] R.W. Pekala, J. Mater. Sci. 24 (9) (1989) 3221–3227.
[6] S.A. Al-Muhtaseb, J.A. Ritter, Adv. Mater. 15 (2) (2003) 101–114.
[7] J. Fricke, R. Petricevic, Handb. Porous Solids 3 (2002) 2037–2062.
[8] M. Glora, M. Wiener, R. Petricevic, H. Pröbstle, J. Fricke, J. Non-Cryst. Solids 285 (1–3) (2001) 283–287.
[9] A. Smirnova, X. Dong, H. Hara, A. Vasiliev, N. Sammes, Int. J. Hydrogen Energy 30 (2) (2005) 149–158.
[10] A. Smirnova, X. Dong, H. Hara, N. Sammes, J. Fuel Cell Sci. Technol. 3 (4) (2006) 477–481.
[11] S.T. Mayer, J.L. Kaschmitter, R.W. Pekala, Carbon aerogel electrodes for direct energy conversion, Application: WO, Regents of the University of California, USA, 1995, 10 pp.
[12] R. Petricevic, G. Reichenauer, V. Bock, A. Emmerling, J. Fricke, J. Non-Cryst. Solids 225 (1) (1998) 41–45.
[13] R. Saliger, V. Bock, R. Petricevic, T. Tillotson, S. Geis, J. Fricke, J. Non-Cryst. Solids 221 (2–3) (1997) 144–150.
[14] R. Petricevic, M. Glora, J. Fricke, Carbon 39 (6) (2001) 857–867.
[15] J. Marie, S. Berthon-Fabry, P. Achard, M. Chatenet, A. Pradourat, E. Chainet, J. Non-Cryst. Solids 350 (2004) 88–96.
[16] P.V. Samant, J.B. Fernandes, C.M. Rangel, J.L. Figueiredo, Catal. Today 102–103 (2005) 173–176.
[17] J.L. Figueiredo, M.F.R. Pereira, P. Serp, P. Kalck, P.V. Samant, J.B. Fernandes, Carbon 44 (12) (2006) 2516–2522.
[18] C. Arbizzani, S. Beninati, E. Manferrari, F. Soavi, M. Mastragostino, J. Power Sources 172 (2) (2007) 578–586.

[19] H. Du, B. Li, F. Kang, R. Fu, Y. Zeng, Carbon 45 (2) (2007) 429–435.
[20] E. Guilminot, F. Fischer, M. Chatenet, A. Rigacci, S. Berthon-Fabry, P. Achard, E. Chainet, J. Power Sources 166 (1) (2007) 104–111.
[21] N. Job, J. Marie, S. Lambert, S. Berthon-Fabry, P. Achard, Energy Convers. Manage. 49 (9) (2008) 2461–2470.
[22] H.-J. Kim, W.-I. Kim, T.-J. Park, H.-S. Park, D.J. Suh, Carbon 46 (11) (2008) 1393–1400.
[23] S. Brunauer, P.H. Emmett, E. Teller, J. Am. Chem. Soc. 60 (2) (1938) 309–319.
[24] B.C. Lippens, J.H. de Boer, J. Catal. 4 (3) (1965) 319–323.
[25] R.S. Mikhail, S. Brunauer, E.E. Bodor, J. Colloid Interf. Sci. 26 (1) (1968) 45–53.
[26] E.P. Barrett, L.G. Joyner, P.P. Halenda, J. Am. Chem. Soc. 73 (1) (1951) 373–380.
[27] M.S. Wilson, J.A. Valerio, S. Gottesfeld, Electrochim. Acta 40 (3) (1995) 355–363.
[28] M.S. Wilson, S. Gottesfeld, J. Appl. Electrochem. 22 (1) (1992) 1–7.
[29] K.R. Cooper, M. Smith, J. Power Sources 160 (2) (2006) 1088–1095.
[30] K.R. Cooper, V. Ramani, J.M. Fenton, H.R. Kunz, Experimental Methods and Data Analyses for Polymer Electrolyte Fuel Cells, Scribner Associates Inc., 2007.
[31] K.S.W. Sing, D.H. Everett, R.A.W. Haul, L. Moscou, R.A. Pierotti, J. Rouquerol, T. Siemieniewska, Pure Appl. Chem. 57 (4) (1985) 603–619.
[32] J.H. Tian, F.B. Wang, Z.Q. Shan, R.J. Wang, J.Y. Zhang, J. Appl. Electrochem. 34 (5) (2004) 461–467.
[33] Z. Zhou, S. Wang, W. Zhou, L. Jiang, G. Wang, G. Sun, B. Zhou, Q. Xin, Phys. Chem. Chem. Phys. 5 (24) (2003) 5485–5488.
[34] J. Appl. Crystallogr. 11 (2) (1978) 102–113.
[35] Z.-H. Teng, G. Wang, B. Wu, Y. Gao, J. Power Sources 164 (1) (2007) 105–110.
[36] http://rsb.info.nih.gov/ij/, accessed August 4, 2009.
[37] T. Vidakovic, M. Christov, K. Sundmacher, Electrochim. Acta 52 (18) (2007) 5606–5613.
[38] A. Pozio, M. De Francesco, A. Cemmi, F. Cardellini, L. Giorgi, J. Power Sources 105 (1) (2002) 13–19.
[39] F. Maillard, S. Schreier, M. Hanzlik, E.R. Savinova, S. Weinkauf, U. Stimming, Phys. Chem. Chem. Phys. 7 (2) (2005) 385–393.
[40] H.A. Gasteiger, S.S. Kocha, B. Sompalli, F.T. Wagner, Appl. Catal. B: Environ. 56 (1–2) (2005) 9–35.
[41] H.A Gasteiger, W. Gu, R. Makharia, M.F. Mathias, B. Sompalli, in: W. Vielstich, H.A. Gasteiger, A. Lamm (Eds.), Handbook of Fuel Cells—Fundamentals, Technology and Applications, John Wiley & Sons, Ltd., 2003.